ORGANIC CHEMISTRY FRONTIERS

RESEARCH ARTICLE

View Article Online
View Journal

Check for updates

Cite this: DOI: 10.1039/d6qo00227g

A polyaromatic dumbbell-based micelle capable of binding large dyes under organic solvent-rich conditions

Lorenzo Catti, * Aguri Sugawara, Kazuki Toyama and Michito Yoshizawa *

Micelles are typical molecular assemblies formed in water. To develop new micelles usable even under organic solvent-rich conditions, we designed and synthesized a dumbbell-shaped polyaromatic amphiphile composed of two bent bisanthracene dimers linked by a long dicationic spacer. The dissolved dumbbells quantitatively assemble into a spherical polyaromatic micelle with a core diameter of ~2 nm in water, exhibiting extremely high stability against dilution (up to 1.2 μM). Through a simple grinding–sonication protocol, organic and metal–organic dyes are efficiently encapsulated by the micelle in water. Strikingly, the resulting host–guest composites retain excellent stability even after addition of a large amount of organic solvent (*e.g.*, 75% v/v methanol), owing to multiple chelate-type π–π and CH–π interactions. The importance of both the long spacer and the dumbbell design is demonstrated by control experiments using an analogous dumbbell possessing a shorter spacer and an amphiphilic semi-dumbbell.

Received 21st February 2026,
Accepted 18th March 2026

DOI: 10.1039/d6qo00227g

rsc.li/frontiers-organic

Open Access Article. Published on 31 March 2026. Downloaded on 4/13/2026 6:57:20 AM.
This article is licensed under a Creative Commons Attribution 3.0 Unported Licence.

Introduction

Micelles, typical molecular assemblies in water, provide both advantages and disadvantages in terms of host functions.[1] One of the advantages is that the size and shape of the host frameworks are widely adaptable to the bound guest molecules, unlike molecular cages and capsules formed from covalent, hydrogen, and/or coordination bonds.[2–4] As a disadvantage, the resultant host–guest composites are unstable in both organic solvents and aqueous organic solvents, owing to facile host dissociation and weak host–guest interactions. There have been many reports on micelles with improved assembly stability in water through covalent linkage of linear alkyl amphiphiles (Fig. 1a).[5,6] However, high stability of micellar host–guest composites against the addition of organic solvent has hardly been realized even using such linked amphiphiles. Our group has developed polyaromatic amphiphile **AA** (Fig. 1b, left and 1c), featuring a bent anthracene dimer with two ionic hydrophilic groups,[7] which generates polyaromatic micelle $(\mathbf{AA})_n$, with relatively strong host abilities, in water.[8] To accomplish high organic solvent compatibility, which can further enhance the practical utility of micelles (*e.g.*, as cleaning and synthetic tools), we designed an amphiphilic polyaromatic dumbbell (Fig. 1b, right), composed of two bent anthracene dimers linked by a single hydrophilic spacer. Here we report (i) the synthesis of **DA** (n = 2, Fig. 1d) and its grinding–sonication-assisted assembly into a new polyaromatic micelle in water and (ii) its high assembly stability against dilution compared to related derivatives, and (iii) the strong binding of various dyes (*e.g.*, fullerene, organic, metal–

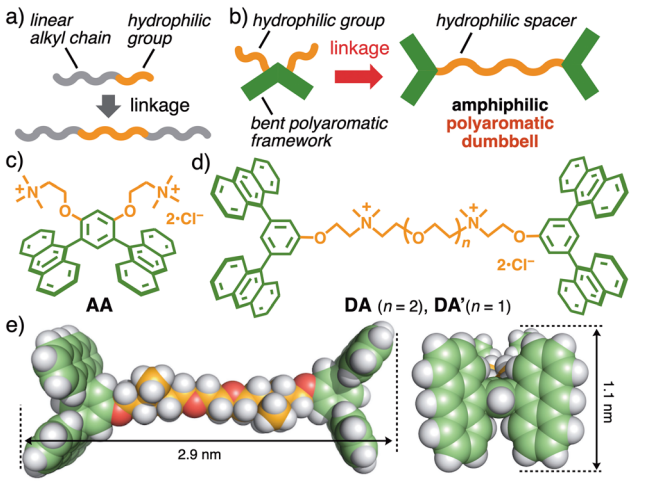

Fig. 1 Linkage of (a) linear alkyl amphiphiles (previous work) and (b) bent polyaromatic amphiphiles (this work), to realize the stabilization of host–guest composites against aqueous organic solvents. (c) Bent polyaromatic amphiphile **AA** reported previously[7] and (d) amphiphilic polyaromatic dumbbells **DA** and **DA'**. (e) Optimized structure (DFT, B3LYP/6-31G(d,p) level) of **DA**: side and bottom views.

Laboratory for Chemistry and Life Science, Institute of Integrated Research, Institute of Science Tokyo, 4259 Nagatsuta, Midori-ku, Yokohama 226-8501, Japan. E-mail: catti.l.aa@m.titech.ac.jp, yoshizawa.m.ac@m.titech.ac.jp

Open Access Article. Published on 31 March 2026. Downloaded on 4/13/2026 6:57:20 AM.
This article is licensed under a Creative Commons Attribution 3.0 Unported Licence.

organic, and polymer dyes) even in organic solvent-rich (up to 75% v/v) aqueous solution.

Polyaromatic micelle $(\mathbf{AA})_n$ possesses wide-ranging encapsulation abilities toward aromatic compounds in water, based on the hydrophobic effect, and efficient π–π and CH–π interactions.[7,8] For the design of a micelle with strong host–guest interactions in aqueous organic media, we incorporated its bent polyaromatic part as the guest binding site into the structure of **DA** (Fig. 1d and e). Two of the bent frameworks were connected on the convex site with a flexible penta(ethylene oxide) spacer embedding two ammonium groups (1.8 nm in length) to enable chelate-type guest binding and reduce repulsive cation–cation interactions within the host.[9] Relocation of the hydrophilic spacer furthermore increased the partial aromatic stackings within **DA** as well as between **DA**s, resulting in improved assembly stability, relative to that of previous micelles formed from amphiphilic polyaromatic oligomers.[10] Analogous dumbbell **DA′** (Fig. 1d), possessing a shorter dicationic spacer (n = 1), and an amphiphilic semi-dumbbell (**VA**) were prepared to study the effect of spacer length and the necessity of the linkage, respectively.

Results and discussion

Formation of the polyaromatic dumbbell-based micelle

Polyaromatic dumbbell-based micelle $(\mathbf{DA})_n$ was quantitatively obtained from amphiphile **DA** dissolved in water *via* grinding–sonication-assisted self-assembly. **DA** was synthesized in five steps starting from 1,3-dibromo-5-methoxybenzene in 26% overall yield (Fig. S1–19).[11] The construction of the bent anthracene dimer by Suzuki–Miyaura coupling and its dimerization through amine quaternization are the key steps. While **DA** (1.2 mg, 1.0 μmol) was virtually insoluble in water (1.0 mL) by simple stirring at room temperature, a clear aqueous solution of micelle $(\mathbf{DA})_n$ (0.4 mM based on **DA**) was obtained through sequential manual grinding (1 min), water addition, sonication (40 kHz, 150 W, 10 min), centrifugation (14 800 rpm, 10 min), and membrane filtration (200 nm pore size; Fig. 2a). Compared to the ^{1}H NMR spectrum of **DA** in $CDCl_3$ (Fig. 2c), that of $(\mathbf{DA})_n$ in D_2O (0.4 mM based on **DA**) showed completely broadened signals ($H_{a–g}$ and $H_{A–F}$), indicating the tight assembly of n·**DA** through the hydrophobic effect and chelate-type, multiple π-stacking interactions (Fig. 2d).[12] The formation of a well-defined assembly with an average core diameter of 1.8 nm in water was indicated by DLS analysis (Fig. 2e). The dry-state AFM analysis also supported the formation of small particles (d = ~1 nm; Fig. 2f and S37).[13] The combination of experimental and molecular modeling studies suggested that the product is on average composed of $(\mathbf{DA})_3$, where the partial inter- and intramolecular stacking of **DA**s generates a spherical polyaromatic core (d = 1.8 nm), surrounded by curved hydrophilic spacers (Fig. 2b). The assembled structure was also supported by UV-visible and fluorescence analyses. The anthracene-based absorption bands of $(\mathbf{DA})_n$ in H_2O were red-shifted ($\Delta\lambda_{max}$ = +7 nm), relative to

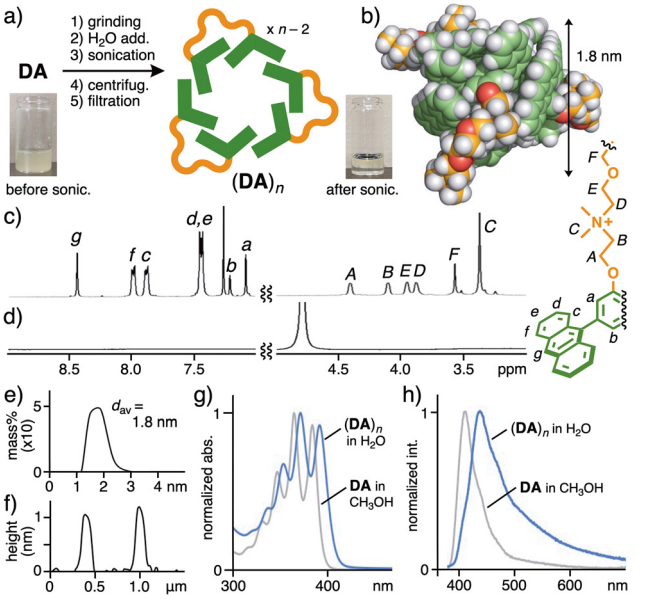

Fig. 2 (a) Selective formation of polyaromatic micelle $(\mathbf{DA})_n$ in water *via* a grinding–sonication protocol. (b) Optimized structure (MM) of $(\mathbf{DA})_3$. ^{1}H NMR spectra (400 MHz, r.t., 0.4 mM based on **DA**) of (c) **DA** in $CDCl_3$ and (d) $(\mathbf{DA})_n$ in D_2O. (e) DLS chart (H_2O, r.t.) of $(\mathbf{DA})_n$ (0.1 mM based on DA) and (f) the AFM-based height profile (dry, r.t., mica) of $(\mathbf{DA})_n$. (g) UV-visible spectra (r.t., 0.4 mM based on **DA**) of $(\mathbf{DA})_n$ in H_2O and **DA** in CH_3OH and (h) their fluorescence spectra (λ_{ex} = 370 nm).

those of monomer **DA** in CH_3OH (λ_{max} = 365 nm, Fig. 2g). The emission band of $(\mathbf{DA})_n$ in H_2O upon excitation at 370 nm was likewise red-shifted ($\Delta\lambda_{max}$ = +29 nm) and broadened, as compared with that of **DA** in CH_3OH (λ_{max} = 414 nm) at the same concentration (Fig. 2h), further suggesting strong π-stacking interactions.

Stability against dilution and the importance of the dumbbell design

The dumbbell-shaped structure of the polyaromatic amphiphile increased the stability of the obtained micelle against water dilution, as evidenced by concentration-dependent fluorescence and NMR analyses. Stepwise dilution of micelle $(\mathbf{DA})_n$ in H_2O (100 to 0.1 μM based on **DA**) resulted in a gradual blue-shift of the emission maximum and decrease in emission intensity at 450 nm (Fig. 3a), owing to gradual disassembly. The corresponding concentration–intensity plot indicated the critical micelle concentration (CMC) of **DA** being 1.2 μM (Fig. 3b).[14] In a similar way, the amphiphilic semi-dumbbell **VA** (Fig. 3d) featuring a single ammonium side-chain assembled into micelle $(\mathbf{VA})_n$ in H_2O, as suggested by NMR, UV-visible, fluorescence, DLS, and molecular modeling analyses (Fig. S20–26 and S39–43). The CMC was estimated to be 50 μM (Fig. 3c and S41),[11] which revealed more than a 40-fold increase in stability upon dimerization. Relative to $(\mathbf{AA})_n$ (CMC = 1 mM),[7] the dilution stability of $(\mathbf{DA})_n$ was thus improved by a factor of ~830, through a combination of facilitated intra/

This journal is © the Partner Organisations 2026

Open Access Article. Published on 31 March 2026. Downloaded on 4/13/2026 6:57:20 AM.
This article is licensed under a Creative Commons Attribution 3.0 Unported Licence.

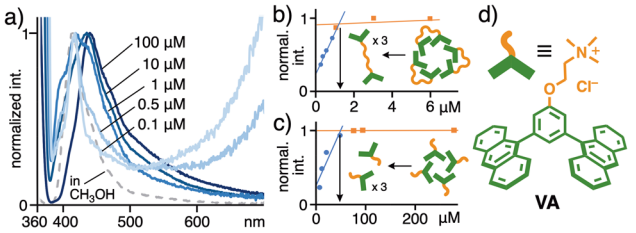

Fig. 3 (a) Concentration-dependent fluorescence spectra (H_2O, r.t., λ_{ex} = 370 nm) of micelle $(\mathbf{DA})_n$ and (b) their concentration *versus* emission intensity plots (λ_{det} = 450 nm). (c) Concentration *versus* emission intensity plots (H_2O, r.t., λ_{ex} = 370 nm, λ_{det} = 480 nm) of $(\mathbf{VA})_n$. (d) Amphiphilic semi-dumbbell **VA**.

intermolecular π–π interactions, reduced electrostatic repulsion, and chelate-type assembly.

The importance of spacer length was verified using the dumbbell derivative **DA′**, which possesses a contracted ethylene oxide spacer (n = 1; Fig. 1d and S27–32). While **DA′** exhibited essentially no solubility in water using the grinding–sonication protocol described above (Fig. S44 and S45), the dissolution and formation of small micelle $(\mathbf{DA}')_n$ (1.0 mM based on **DA′**), with an average core diameter of 1.3 nm, was observed in a 1 : 1 H_2O/CH_3OH mixture, as indicated by UV-visible and DLS analyses (Fig. 4a). The UV-visible spectrum suggested the assembly, due to a red-shift of the anthracene-based absorption band of **DA′** ($\Delta\lambda_{max}$ = +4 nm), as compared to that in CH_3OH (Fig. 4b). The emission band of $(\mathbf{DA}')_n$ at λ_{max} = 478 nm upon irradiation at 370 nm was also red-shifted by +60 nm relative to that of monomer **DA′** in CH_3OH (Fig. 4c). On the basis of these findings, molecular modeling studies suggested the assembly of **DA′** into dimer $(\mathbf{DA}')_2$ in a π-stacked, face-to-face fashion, even in the presence of 50% v/v CH_3OH (Fig. 4d, e and S47).[15]

Dye binding under organic solvent-rich conditions

Besides the high stability of micelle $(\mathbf{DA})_n$ against water dilution, the efficient formation of its host–guest composites and their high stability against the addition of organic solvent were revealed in the following studies. Fullerene C_{60} ($\mathbf{C_{60}}$) was used as a typical hydrophobic dye and a mixture of **DA** (0.9 mg, 0.8 μmol) and $\mathbf{C_{60}}$ (0.1 mg, 0.2 μmol) was ground for 1 min using an agate mortar and pestle (Fig. 5a). After the addition of H_2O (2.5 mL), the suspension was sonicated with a probe sonicator (40 kHz, 150 W, 10 min, 0 °C), centrifuged, and filtered to give a clear brown solution containing host–guest composite $(\mathbf{DA})_n{\cdot}(\mathbf{C_{60}})_m$. The product size and composition were revealed by a combination of DLS (*i.e.*, 2.3 nm in diameter; Fig. S49a), UV-visible, and molecular modeling analyses (*i.e.*, $n : m$ = 3 : 1; Fig. S49b).[11] The efficient encapsulation of $\mathbf{C_{60}}$ was confirmed by the UV-visible analysis. On the basis of the intensity of new absorption bands (λ = 440 nm) derived from encapsulated $(\mathbf{C_{60}})_m$, the uptake ability of $(\mathbf{DA})_n$ was slightly lower than that of $(\mathbf{AA})_n$ under the same conditions (0.8-fold; Fig. 5c, d, and S48). Next, methanol (1.5 mL) was added to $(\mathbf{DA})_n{\cdot}(\mathbf{C_{60}})_m$ in H_2O (0.5 mL, 0.3 mM based on **DA**) at room temperature (Fig. 5b) and the resultant pale brown solution (75% v/v methanol, 75 μM based on **DA**) was again analyzed by UV-visible spectroscopy after centrifugation and filtration.[16] The spectrum was nearly identical to that of $(\mathbf{DA})_n{\cdot}(\mathbf{C_{60}})_m$ in H_2O (75 μM based on **DA**; Fig. 5c). The relative retention efficiency of the host–guest composite was estimated to be ~100% (Fig. 5e), from the intensity change in the guest band at 440 nm. The band intensity of the diluted solution was nearly unchanged (82% retention) at room temperature even after 1 month (Fig. S51c), revealing excellent stability against methanol dilution.

In sharp contrast, the $\mathbf{C_{60}}$-based absorption bands of $(\mathbf{AA})_n{\cdot}(\mathbf{C_{60}})_m$ and $(\mathbf{VA})_n{\cdot}(\mathbf{C_{60}})_m$ in water (150 μM based on **AA** and **VA**) decreased upon addition of methanol (Fig. 5d and S50a),

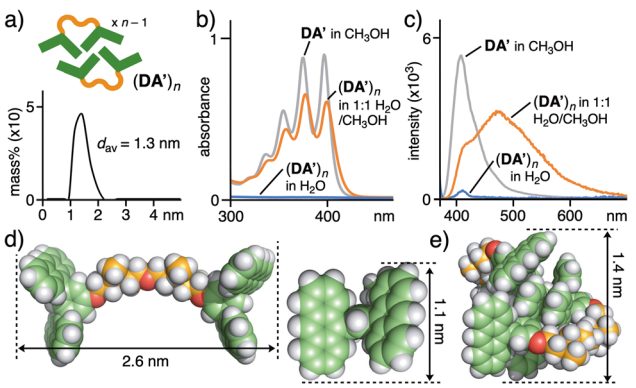

Fig. 4 (a) DLS chart (1 : 1 H_2O/CH_3OH, r.t., 0.1 mM based on DA′) of micelle $(\mathbf{DA}')_n$. (b) UV-visible spectra (r.t., 0.4 mM based on DA′) of $(\mathbf{DA}')_n$ in H_2O and 1 : 1 H_2O/CH_3OH, and **DA′** in CH_3OH and (c) their fluorescence spectra (λ_{ex} = 370 nm). Optimized structures of (d) **DA′** (front and bottom views) and (e) $(\mathbf{DA}')_2$ (DFT, B3LYP/6-31G(d,p) level and MM, respectively).

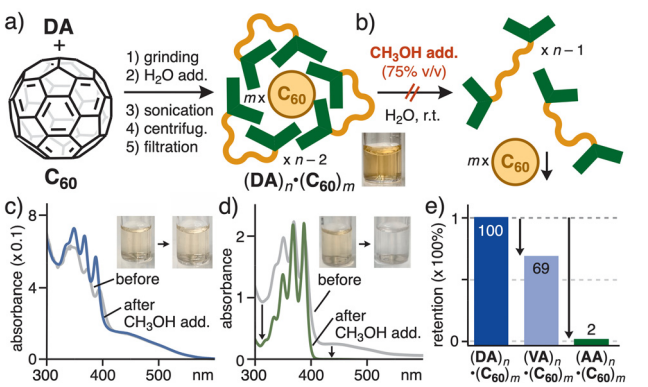

Fig. 5 (a) Encapsulation of $\mathbf{C_{60}}$ by micelle $(\mathbf{DA})_n$ in water and (b) stability of host–guest composite $(\mathbf{DA})_n{\cdot}(\mathbf{C_{60}})_m$ against CH_3OH dilution. UV-visible spectra (r.t., 75/150 μM based on DA/AA, 1 cm path-length quartz cell) of (c) $(\mathbf{DA})_n{\cdot}(\mathbf{C_{60}})_m$ and (d) $(\mathbf{AA})_n{\cdot}(\mathbf{C_{60}})_m$ before and 1 h after the addition of CH_3OH (75% v/v). (e) Relative stabilities of (**DA** or **VA** or $\mathbf{AA})_n{\cdot}(\mathbf{C_{60}})_m$ in water after CH_3OH addition.

Open Access Article. Published on 31 March 2026. Downloaded on 4/13/2026 6:57:20 AM.
This article is licensed under a Creative Commons Attribution 3.0 Unported Licence.

owing to the release of bound m·**C_{60}**, under the same conditions. Their retention efficiencies were estimated to be 2% and 69% after 1 h, respectively (Fig. 5e). Typical alkyl amphiphiles (*i.e.*, sodium dodecyl sulfate (**SDS**)) showed poor uptake abilities toward **C_{60}** and no retention abilities toward the bound **C_{60}** under the same conditions (Fig. S52).[11] Host–guest composite (**DA**)$_n$·(**C_{60}**)$_m$ also showed high stability against the addition of DMSO, acetone, and acetonitrile (75% v/v each), with the retention efficiencies being ~100%, 97%, and 99%, respectively (Fig. S50b). Similar encapsulation and retention (~100%) were also observed for higher fullerene C_{70} by using (**DA**)$_n$ under the same conditions (Fig. S53). These results indicated that both the bent polyaromatic frameworks and the connected hydrophilic chain of **DA** are of importance for tight host–guest interactions under organic solvent-rich aqueous conditions.

High stability against methanol-rich conditions was also demonstrated for host–guest composites containing organic and metal–organic dyes as well as polymer dyes. Subjecting **DA** (0.9 mg, 0.8 μmol) and rubrene (**Rub**; 0.1 mg, 0.2 μmol) to the established grinding–sonication protocol yielded a clear red solution containing (**DA**)$_n$·(**Rub**)$_m$ (Fig. 6a and c). The obtained UV-visible spectrum of the aqueous solution exhibited new dye-derived absorption bands at 400–560 nm, which remained largely unchanged (94% retention) upon the 75% v/v addition of methanol (Fig. 6d). On the other hand, 43% and no retention of **Rub** were observed in the case of (**VA**)$_n$ and (**AA**)$_n$ under similar conditions, respectively. To elucidate the structural origin of the high stability of (**DA**)$_n$·(**Rub**)$_m$, the **DA** : **Rub** ratio was determined to be 4 : 5 by the ^{1}H NMR integral analysis of the isolated host–guest composite in $CDCl_3$, facilitated by sufficient solubility of both **DA** and **Rub** in this solvent (Fig. S55). In combination with the DLS-derived particle diameter of 4.9 nm on average (Fig. 6e), molecular modeling analyses indicated the formation of (**DA**)$_8$·(**Rub**)$_{10}$ as the main species in solution (Fig. 6f). In the structure, roughly spherical aggregate (**Rub**)$_{10}$ is fully enclosed by the sixteen polyaromatic panels of eight **DA**s, stabilized through multiple π–π and CH–π interactions.

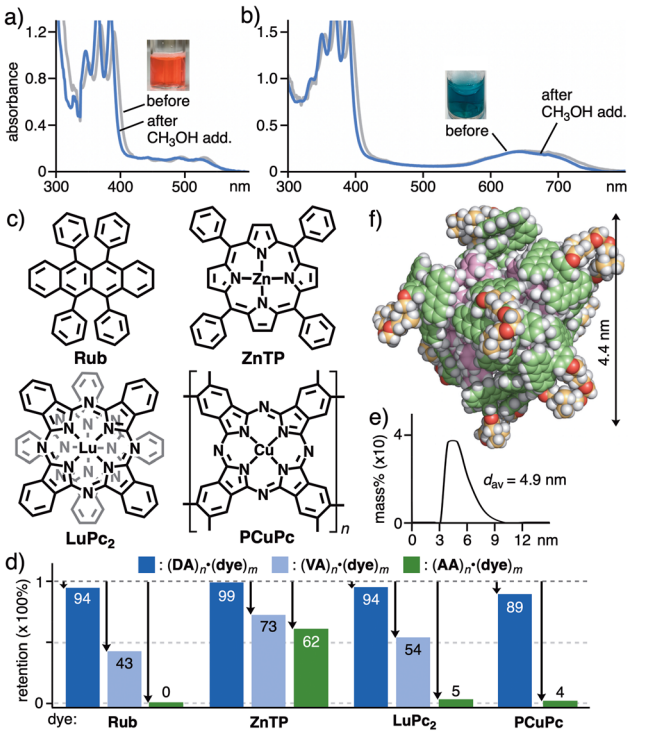

Fig. 6 UV-visible spectra (r.t., 75 μM based on **DA**, 1 cm path-length quartz cell) of (a) (**DA**)$_n$·(**Rub**)$_m$ and (b) (**DA**)$_n$·(**PCuPc**)$_m$ before and after the addition of CH_3OH (75% v/v). (c) Organic and metal-complex dyes **Rub**, **ZnTP**, **LuPc$_2$**, and **PCuPc**. (d) Relative stabilities of (**DA** or **VA** or **AA**)$_n$·(**dye**)$_m$ in water after CH_3OH addition. (e) DLS chart (H_2O, r.t., 0.1 mM based on **DA**) of (**DA**)$_n$·(**Rub**)$_m$. (f) Optimized structure (MM) of (**DA**)$_8$·(**Rub**)$_{10}$.

Metal–organic dyes such as Zn(II)-tetraphenylporphyrin (**ZnTP**) and Lu(II)-bisphthalocyaninato (**LuPc$_2$**; Fig. 6c) were encapsulated by (**DA**)$_n$ (Fig. S57 and S58). The retention efficiencies upon 75% v/v methanol addition were estimated to be 99% and 94% for **DA**, 73% and 54% for **VA**, and 62% and 5% for **AA**, respectively (Fig. 6d). Notably, metal–organic polymer dyes, *i.e.*, poly-Cu(II)-phthalocyanines (**PCuPc**; Fig. 6c) were also effectively encapsulated and retained (89%) upon methanol addition, as judged by the broad dye-derived absorption band at 550–750 nm in the UV-visible spectra (Fig. 6b and d). In contrast, **PCuPc** was hardly encapsulated by (**VA**)$_n$ in water and nearly all of **PCuPc** was released from (**AA**)$_n$·(**PCuPc**)$_m$ upon methanol addition (Fig. 6d and S60). Host–guest composites derived from (**DA**)$_n$ and polythiophenes (**PT**) as organic polymer dyes likewise exhibited high stability under methanol-rich conditions (Fig. S61). The above results highlight the host function of (**DA**)$_n$ toward various dyes as well as the high dye retention abilities in methanol-rich solution.

Conclusions

We have designed and prepared a new micelle with high stability and high dye-binding ability under organic solvent-rich conditions. Amphiphilic polyaromatic dumbbells, featuring two bent anthracene dimers linked by a long flexible spacer, quantitatively assembled in water into a spherical polyaromatic micelle composed of three dumbbells on average. The micelle exhibited extremely high stability against dilution (up to 1.2 μM), around 830-fold higher compared to a non-dumbbell-based polyaromatic micelle. Various organic and metal–organic dyes were efficiently encapsulated by the micelle in water. Importantly, the corresponding host–guest composites showed unusually high stability against the addition of a large amount of organic solvent (75% v/v; *e.g.*, methanol, DMSO, and acetone), with the aid of the hydrophobic effect and multiple chelate-type π–π and CH–π interactions. We anticipate that the present "organostable" micelle will enable new host functions not only in water but also in aqueous organic

This journal is © the Partner Organisations 2026

Open Access Article. Published on 31 March 2026. Downloaded on 4/13/2026 6:57:20 AM. This article is licensed under a Creative Commons Attribution 3.0 Unported Licence.

solvent media, *e.g.*, for applications in painting materials, extraction/separation tools, and catalysis.

Author contributions

L. C., A. S., K. T, and M. Y. designed the work, carried out research, analyzed data, and wrote the paper. All authors discussed the results and commented on the manuscript.

Conflicts of interest

There are no conflicts to declare.

Data availability

The data supporting this article have been included as part of the supplementary information (SI). Supplementary information is available. Experimental procedures, and NMR, MS, UV-visible, emission, AFM, DLS, and theoretical data. See DOI: **https://doi.org/10.1039/d6qo00227g**.

Acknowledgements

This work was supported by JSPS KAKENHI (Grant No. JP22H00348/JP23K17913/JP22H05560/JP23K13760/JP23KK0127/JP24H01311). Theoretical calculations were performed using computers at the Research Center for Computational Science, Okazaki, Japan (23-IMS-C063, 24-IMS-C060). K. T. acknowledges JST SPRING (Grant No. JPMJSP2106) and JSPS Research Fellowship for Young Scientists (Grant No. 25KJ1257).

References

1 (*a*) Y. Moroi, *Micelles: Theoretical and Applied Aspects*, Plenum, New York, 1992; (*b*) T. F. Tadros, *Applied Surfactants: Principles and Applications*, Wiley-VCH, Weinheim, 2005; (*c*) D. Myers, *Surfactant Science and Technology*, Wiley, Hoboken, 2006.

2 Covalent hosts: (*a*) T. Ogoshi, T. Yamagishi and Y. Nakamoto, Pillar-Shaped Macrocyclic Hosts Pillar[*n*]arenes: New Key Players for Supramolecular Chemistry, *Chem. Rev.*, 2016, **116**, 7937–8002; (*b*) Z. Liu, S. K. M. Nalluri and J. F. Stoddart, Surveying macrocyclic chemistry: from flexible crown ethers to rigid cyclophanes, *Chem. Soc. Rev.*, 2017, **46**, 2459–2478; (*c*) L. Escobar and P. Ballester, Molecular Recognition in Water Using Macrocyclic Synthetic Receptors, *Chem. Rev.*, 2021, **121**, 2445–2514; (*d*) G. Montà-González, F. Sancenón, R. Martínez-Máñez and V. Martí-Centelles, Purely Covalent Molecular Cages and Containers for Guest Encapsulation, *Chem. Rev.*, 2022, **122**, 13636–13708; (*e*) C. J. T. Cox, J. Hale, P. Molinska and J. E. M. Lewis, Supramolecular and molecular capsules, cages and containers, *Chem. Soc. Rev.*, 2024, **53**, 10380–10408.

3 Hydrogen-bonding hosts: (*a*) L. Adriaenssens and P. Ballester, Hydrogen bonded supramolecular capsules with functionalized interiors: the controlled orientation of included guests, *Chem. Soc. Rev.*, 2013, **42**, 3261–3277; (*b*) Q. Zhang, L. Catti and K. Tiefenbacher, Catalysis inside the Hexameric Resorcinarene Capsule, *Acc. Chem. Res.*, 2018, **51**, 2107–2114; (*c*) Y. Yu and J. Rebek Jr., Reactions of Folded Molecules in Water, *Acc. Chem. Res.*, 2018, **51**, 3031–3040.

4 Coordination hosts: (*a*) E. G. Percástegui, T. K. Ronson and J. R. Nitschke, Design and Applications of Water-Soluble Coordination Cages, *Chem. Rev.*, 2020, **120**, 13480–13544; (*b*) S. Pullen, J. Tessarolo and G. H. Clever, Increasing structural and functional complexity in self-assembled coordination cages, *Chem. Sci.*, 2021, **12**, 7269–7293; (*c*) H. Takezawa and M. Fujita, Molecular Confinement Effects by Self-Assembled Coordination Cages, *Bull. Chem. Soc. Jpn.*, 2021, **94**, 2351–2369; (*d*) W. Liu and J. F. Stoddart, Emergent behavior in nanoconfined molecular containers, *Chem*, 2021, **7**, 919–947; (*e*) R. Banerjee, D. Chakraborty and P. S. Mukherjee, Molecular Barrels as Potential Hosts: From Synthesis to Applications, *J. Am. Chem. Soc.*, 2023, **145**, 7692–7711; (*f*) R. Ham, C. J. Nielsen, S. Pullen and J. N. H. Reek, Supramolecular Coordination Cages for Artificial Photosynthesis and Synthetic Photocatalysis, *Chem. Rev.*, 2023, **123**, 5225–5261.

5 Gemini amphiphiles: (*a*) F. M. Menger and J. S. Keiper, Gemini Surfactants, *Angew. Chem., Int. Ed.*, 2000, **39**, 1906–1920; (*b*) M. Dekker, *Gemini Surfactants, Synthesis Interfacial and Solution-Phase Behavior, and Applications*, CRC Press, New York, 2003.

6 An oligoaromatic dumbbell-shaped amphiphile forming toroid assemblies in water; J.-K. Kim, E. Lee, Z. Huang and M. Lee, Nanorings from the Self-Assembly of Amphiphilic Molecular Dumbbells, *J. Am. Chem. Soc.*, 2006, **128**, 14022–14023.

7 K. Kondo, A. Suzuki, M. Akita and M. Yoshizawa, Micelle-like Molecular Capsules with Anthracene Shells as Photoactive Hosts, *Angew. Chem., Int. Ed.*, 2013, **52**, 2308–2312.

8 Reviews and recent works: (*a*) M. Yoshizawa and L. Catti, Bent Anthracene Dimers as Versatile Building Blocks for Supramolecular Capsules, *Acc. Chem. Res.*, 2019, **52**, 2392–2404; (*b*) M. Yoshizawa and L. Catti, Aromatic micelles: toward a third-generation of micelles, *Proc. Jpn. Acad., Ser. B*, 2023, **99**, 29–38; (*c*) S. Aoyama, L. Catti and M. Yoshizawa, Facile Processing of Unsubstituted π-Conjugated Aromatic Polymers through Water-solubilization Using Aromatic Micelles, *Angew. Chem., Int. Ed.*, 2023, **62**, e202306399; (*d*) L. Catti, S. Aoyama and M. Yoshizawa, Facile access to pyridinium-based bent aromatic amphiphiles: nonionic surface modification of nanocarbons in water, *Beilstein J. Org. Chem.*, 2024, **20**, 32–40; (*e*) M. Endo, S. Aoyama, Y. Tsuchido, L. Catti and

Open Access Article. Published on 31 March 2026. Downloaded on 4/13/2026 6:57:20 AM.
This article is licensed under a Creative Commons Attribution 3.0 Unported Licence.

M. Yoshizawa, Umbrella-Shaped Amphiphiles: Internal Alkylation of an Aromatic Micelle and Its Impact on Cavity Features, *Angew. Chem., Int. Ed.*, 2024, **63**, e202404088; (*f*) L. Catti, S. Yasugami, S. Aoyama, N. Kishida and M. Yoshizawa, A Photolockable Polyaromatic Capsule Designed via Regiochemical Substitution, *Chem. – Eur. J.*, 2025, **31**, e202403703; (*g*) S. Aoyama, L. Catti and M. Yoshizawa, Aqueous polycavity hosts composed of porous aromatic polymers within aromatic micelles, *Chem*, 2025, **11**, 102616; (*h*) D. Kidoh, L. Catti, S. Aoyama, D. Tauchi, M. Hasegawa and M. Yoshizawa, Hybridized Host Functions in Polyaromatic Tube-in-Capsule Composites, *Angew. Chem., Int. Ed.*, 2026, **65**, e21942; (*i*) Y. Kikuchi, L. Catti, S. Aoyama, T. Sawada and M. Yoshizawa, Construction of Well-Defined Yet Adaptable Oligo(Amino Acid) Cavities within an Aromatic Micelle, *J. Am. Chem. Soc.*, 2026, **148**, 1034–1040.

9 The lower charges per anthracene panel ratio results in reduced electrostatic repulsion between the amphiphiles and an increased solvophobic effect (*i.e.*, anthracene panel/charge = 2 (**DA**) and 1 (**AA**)).

10 (*a*) T. Nishioka, K. Kuroda, M. Akita and M. Yoshizawa, A Polyaromatic Gemini Amphiphile That Assembles into a Well-Defined Aromatic Micelle with Higher Stability and Host Functions, *Angew. Chem., Int. Ed.*, 2019, **58**, 6579–6583; (*b*) Y. Tsuchida, K. Aratsu, S. Hiraoka and M. Yoshizawa, An Aromatic Oligomer Micelle: Large Enthalpic Stabilization and Selective Oligothiophene Uptake, *Angew. Chem., Int. Ed.*, 2021, **60**, 12754–12758.

11 See the SI. Chloride counter anions were used for the amphiphiles due to the insolubility of the corresponding iodide salts in water.

12 The saturated concentration of $(\mathbf{DA})_n$ in water was estimated to be 0.4 mM based on **DA** through the UV-visible study.

13 The observed smaller dimensions most probably arise from the strong interactions between the less protected, polyaromatic framework of $(\mathbf{DA})_n$ and the mica surface.

14 The concentration-dependent ^{1}H NMR analysis also indicated the CMC being less than 50 μM in water, owing to the highly broadened signals (Fig. S33c).[11]

15 Aromatic micelle $(\mathbf{DA}')_n$ encapsulated fullerene $\mathbf{C_{60}}$ in a 1 : 1 mixture of H_2O/CH_3OH, albeit with a lower efficiency than **DA** and **VA**.

16 The assembled structure of $(\mathbf{DA})_n$ remained mostly intact in 25 : 75 D_2O/CD_3OD (0.1 mM based on **DA**) at room temperature as estimated by ^{1}H NMR analysis (Fig. S33d).

This journal is © the Partner Organisations 2026